Six centuries of variability and extremes in a coupled marine-terrestrial ecosystem

Bryan A. Black *et al.*

Science **345**, 1498 (2014);
DOI: 10.1126/science.1253209

valenced events (*21*) via its basal ganglia inputs (*22*), and its hyperexcitation may contribute to human depression (*16*, *38*). We found that co-release of GABA and glutamate occurs in the LHb and that the opponent actions of these neurotransmitters control the level of LHb activity by basal ganglia inputs. Our studies identify an unusual form of inhibition controlling the activity of this key brain region.

There is physiological evidence for co-release of GABA and glutamate (*3*) in the auditory system (*5*) and CA3 region of the hippocampus (*4*, *6*–*8*), where it may contribute to refinement of neuronal connectivity during development (*6*, *39*) and be induced by seizures in the adult hippocampus (*11*); GABA and glutamate co-release has not been universally accepted (*10*). Here, we show using a combination of electrophysiological, optogenetic, mouse genetic, and fluorescent and EM immunohistochemical techniques that in the adult rodent brain a substantial fraction of EP inputs to the LHb simultaneously release both glutamate and GABA and that these neurotransmitters have opposite effects on postsynaptic spike output. Co-release of glutamate and GABA can permit very local control, at the level of individual presynaptic terminals, in the balance of excitation and inhibition, a key mechanism controlling neuronal excitability (*1*).

The LHb receives long-range excitatory and inhibitory inputs from several sources (*40*–*42*). It remains to be determined whether other inputs to the LHb co-release glutamate and GABA and the extent to which co-release of glutamate and GABA is used to regulate excitability in the rest of the nervous system (*3*). Co-expression of Vglut2 and GAD mRNA has been found in EP neurons that project to the motor thalamus, suggesting that co-release of glutamate and GABA may also occur in this pathway (*43*).

Given the proposed role of increased neuronal activity in the LHb in mood disorders (*16*), we examined the ratio of GABA to glutamate released at the EP-LHb synapse in conditions related to depression. In animals chronically treated with citalopram, a drug used to treat depression, evidence indicated enhanced GABA at EP-LHb synapses. In line with these data, EP-LHb synapses in cLH rats, which model aspects of human depression, showed evidence of reduced GABA, although additional changes (e.g., in receptor number) cannot be ruled out. Our results identify co-release of GABA and glutamate as a regulator of LHb output and potential determinant of the impact of negatively valenced events on mood and behavior.

REFERENCES AND NOTES

1. J. S. Isaacson, M. Scanziani, *Neuron* **72**, 231–243 (2011).
2. K. Brinschwitz *et al*., *Neuroscience* **168**, 463–476 (2010).
3. R. P. Seal, R. H. Edwards, *Curr. Opin. Pharmacol.* **6**, 114–119 (2006).
4. M. C. Walker, A. Ruiz, D. M. Kullmann, *Neuron* **29**, 703–715 (2001).
5. D. C. Gillespie, G. Kim, K. Kandler, *Nat. Neurosci.* **8**, 332–338 (2005).
6. J. Q. Beltrán, R. Gutiérrez, *J. Physiol.* **590**, 4789–4800 (2012).
7. C. Cabezas, T. Irinopoulou, G. Gauvain, J. C. Poncer, *J. Neurosci.* **32**, 11835–11840 (2012).
8. V. F. Safiulina, G. Fattorini, F. Conti, E. Cherubini, *J. Neurosci.* **26**, 597–608 (2006).
9. M. D. Caiati, *J. Neurosci.* **33**, 1755–1756 (2013).
10. M. Uchigashima, M. Fukaya, M. Watanabe, H. Kamiya, *J. Neurosci.* **27**, 8088–8100 (2007).
11. R. Gutiérrez, *Trends Neurosci.* **28**, 297–303 (2005).
12. J. Shumake, E. Edwards, F. Gonzalez-Lima, *Brain Res.* **963**, 274–281 (2003).
13. S. Caldecott-Hazard, J. Mazziotta, M. Phelps, *J. Neurosci.* **8**, 1951–1961 (1988).
14. B. Li *et al*., *Nature* **470**, 535–539 (2011).
15. K. Li *et al*., *Science* **341**, 1016–1020 (2013).
16. A. Sartorius *et al*., *Biol. Psychiatry* **67**, e9–e11 (2010).
17. C. Winter, B. Vollmayr, A. Djodari-Irani, J. Klein, A. Sartorius, *Behav. Brain Res.* **216**, 463–465 (2011).
18. J. S. Morris, K. A. Smith, P. J. Cowen, K. J. Friston, R. J. Dolan, *Neuroimage* **10**, 163–172 (1999).
19. J. Amat *et al*., *Brain Res.* **917**, 118–126 (2001).
20. N. Eshel, J. P. Roiser, *Biol. Psychiatry* **68**, 118–124 (2010).
21. M. Matsumoto, O. Hikosaka, *Nature* **447**, 1111–1115 (2007).
22. S. Hong, O. Hikosaka, *Neuron* **60**, 720–729 (2008).
23. G. C. Patton, C. Coffey, M. Posterino, J. B. Carlin, G. Bowes, *Psychol. Med.* **33**, 1203–1210 (2003).
24. E. S. Boyden, F. Zhang, E. Bamberg, G. Nagel, K. Deisseroth, *Nat. Neurosci.* **8**, 1263–1268 (2005).
25. S. J. Shabel, C. D. Proulx, A. Trias, R. T. Murphy, R. Malinow, *Neuron* **74**, 475–481 (2012).
26. Materials and methods are available as supplementary material on *Science* Online.
27. L. Vong *et al*., *Neuron* **71**, 142–154 (2011).
28. H. C. Tsai *et al*., *Science* **324**, 1080–1084 (2009).
29. S. Melzer *et al*., *Science* **335**, 1506–1510 (2012).
30. E. C. Fuchs *et al*., *Proc. Natl. Acad. Sci. U.S.A.* **98**, 3571–3576 (2001).
31. S. Tolu *et al*., *FASEB J.* **24**, 723–730 (2010).
32. H. Tokuno, T. Moriizumi, M. Kudo, Y. Kitao, Y. Nakamura, *Brain Res.* **474**, 390–393 (1988).
33. S. Caldecott-Hazard, *Exp. Neurol.* **99**, 73–83 (1988).
34. J. Hyttel, *Prog. Neuropsychopharmacol. Biol. Psychiatry* **6**, 277–295 (1982).
35. U. Freo, C. Ori, M. Dam, A. Merico, G. Pizzolato, *Brain Res.* **854**, 35–41 (2000).
36. J. Jarosik, B. Legutko, K. Unsicker, O. von Bohlen Und Halbach, *Exp. Neurol.* **204**, 20–28 (2007).
37. B. Vollmayr *et al*., *Behav. Brain Res.* **150**, 217–221 (2004).
38. O. Hikosaka, *Nat. Rev. Neurosci.* **11**, 503–513 (2010).
39. J. Noh, R. P. Seal, J. A. Garver, R. H. Edwards, K. Kandler, *Nat. Neurosci.* **13**, 232–238 (2010).
40. A. M. Stamatakis *et al*., *Neuron* **80**, 1039–1053 (2013).
41. M. Herkenham, W. J. Nauta, *J. Comp. Neurol.* **173**, 123–145 (1977).
42. Z. Gottesfeld, V. J. Massari, E. A. Muth, D. M. Jacobowitz, *Brain Res.* **130**, 184–189 (1977).
43. P. Barroso-Chinea *et al*., *Neurobiol. Dis.* **31**, 422–432 (2008).

ACKNOWLEDGMENTS

We thank H. Monyer and O. Kiehn for transgenic mice, R. Edwards for Vglut2 antibodies and DNA, K. Deisseroth for ChR2 DNA, J. Lin and R. Tsien for oChiEf DNA, T. Meerloo for electron microscopy assistance, and V. Joseph for histology assistance. We thank N. Spitzer and J. Issaacson and the Malinow laboratory for helpful suggestions. This work was supported by an NIH grant to R.M. awarded to the University of California, San Diego (UCSD) Neuroscience Core (NS047101). C.D.P was supported by a postdoctoral award by the Instituts de Recherche en Santé du Canada. All primary electrophysiological and immunohistochemical data are archived in the Center for Neural Circuits and Behavior at UCSD.

SUPPLEMENTARY MATERIALS

www.sciencemag.org/content/345/6203/1494/suppl/DC1
Materials and Methods
Figs. S1 to S23
References (*44*, *45*)

6 January 2014; accepted 5 August 2014
10.1126/science.1250469

CLIMATE CHANGE

Six centuries of variability and extremes in a coupled marine-terrestrial ecosystem

Bryan A. Black,[1]* William J. Sydeman,[2] David C. Frank,[3] Daniel Griffin,[4] David W. Stahle,[5] Marisol García-Reyes,[6] Ryan R. Rykaczewski,[7] Steven J. Bograd,[8] William T. Peterson[9]

Reported trends in the mean and variability of coastal upwelling in eastern boundary currents have raised concerns about the future of these highly productive and biodiverse marine ecosystems. However, the instrumental records on which these estimates are based are insufficiently long to determine whether such trends exceed preindustrial limits. In the California Current, a 576-year reconstruction of climate variables associated with winter upwelling indicates that variability increased over the latter 20th century to levels equaled only twice during the past 600 years. This modern trend in variance may be unique, because it appears to be driven by an unprecedented succession of extreme, downwelling-favorable, winter climate conditions that profoundly reduce productivity for marine predators of commercial and conservation interest.

In coastal upwelling zones, alongshore equatorward winds lift deep, cold, nutrient-rich waters into sunlit surface layers, fueling vast phytoplankton blooms that ultimately support large resident and migratory populations of fish, seabirds, and marine mammals (*1*, *2*). These systems are characterized by considerable interannual to multidecadal variability, including, in some locations, long-term linear trends in upwelling intensity (*3*). However, observational records rarely span more than 70 years, hindering the ability to identify underlying forcing mechanisms or to assess whether these patterns are exceptional over multicentennial time scales.

In the California Current (CC) upwelling zone along the west coast of North America, ecosystem

function may be critically dependent on cool (winter)–season marine climate (*4*). Wintertime upwelling intensity, the variability of which is a function of winter sea-level pressure (SLP) over the northeast Pacific [i.e., the North Pacific High (NPH)], synchronizes independent upper-trophic indicators, including rockfish (*Sebastes* spp.) growth and seabird reproductive success (*5*–*7*). The same atmospheric conditions that control winter upwelling and associated marine productivity also control onshore precipitation and tree growth by facilitating or blocking storm access to western North America (*8*). We capitalized on the tight coupling between the oceanic and terrestrial systems to generate a tree-ring reconstruction of CC winter marine climate spanning almost 600 years.

Three physical variables were used to characterize CC winter climate: (i) the Northern Oscillation Index [NOI, an index of the NPH (*9*)], (ii) the Bakun Upwelling Index (*10*), and (iii) sea level at San Francisco (SFO). The Upwelling Index and sea level provide a regional CC perspective to complement the broad-scale NOI. All three variables are highly correlated. The offshore high-pressure systems drive northerly upwelling-favorable winds that depress coastal sea levels (Fig. 1, fig. S1, and table S1). The first principal component of the three winter (January to March) instrumental variables (Upwelling Index averaged across 36° and 39°N, SFO sea level, and the NOI) captures 85% of the variability and serves as a multivariate index of marine climate (the California Current Winter Index; CCWI), the target of our reconstruction. The CCWI is negatively correlated with precipitation from central to southern California (Fig. 1 and table S1). Thus, California drought is associated with a strong NPH (positive NOI), robust upwelling, and low sea level (fig. S1).

Biological time series in the CC and adjacent terrestrial ecosystems closely track the CCWI. Among tree-ring chronologies in western North America, significant ($P < 0.01$) correlations with the CCWI are concentrated in California and are exclusively negative (Fig. 1). Because of their length and strong covariation with winter precipitation (*8*, *11*), we used blue oak (*Quercus douglasii*) tree-ring chronologies to develop our reconstruction. Chronologies that contained at least three trees >400 years old, were sampled after 2002, and correlate to the CCWI at the $P < 0.001$ level were used in the analyses ($n = 16$). In the marine ecosystem, we focused on four biological time series because of their length (>35 years), spatial overlap, and understood responses to winter climate (*5*, *6*). The records include the otolith growth-increment chronology spanning 1948–2006 for splitnose rockfish (*Sebastes diploproa*; valid for 36° to 39°N), mean egg-laying dates for the seabirds Cassin's auklet (*Ptychoramphus aleuticus*) and common murre (*Uria aalge*), and the breeding success of the common murre (seabird records span 1972–2006).

The first principal component of the four marine biological time series ($PC1_{bio}$; 1972–2003) and the average of the 16 blue oak chronologies capture 67% of the total variance among these indicators. PC loadings highlight inverse productivity between the marine and terrestrial ecosystems;

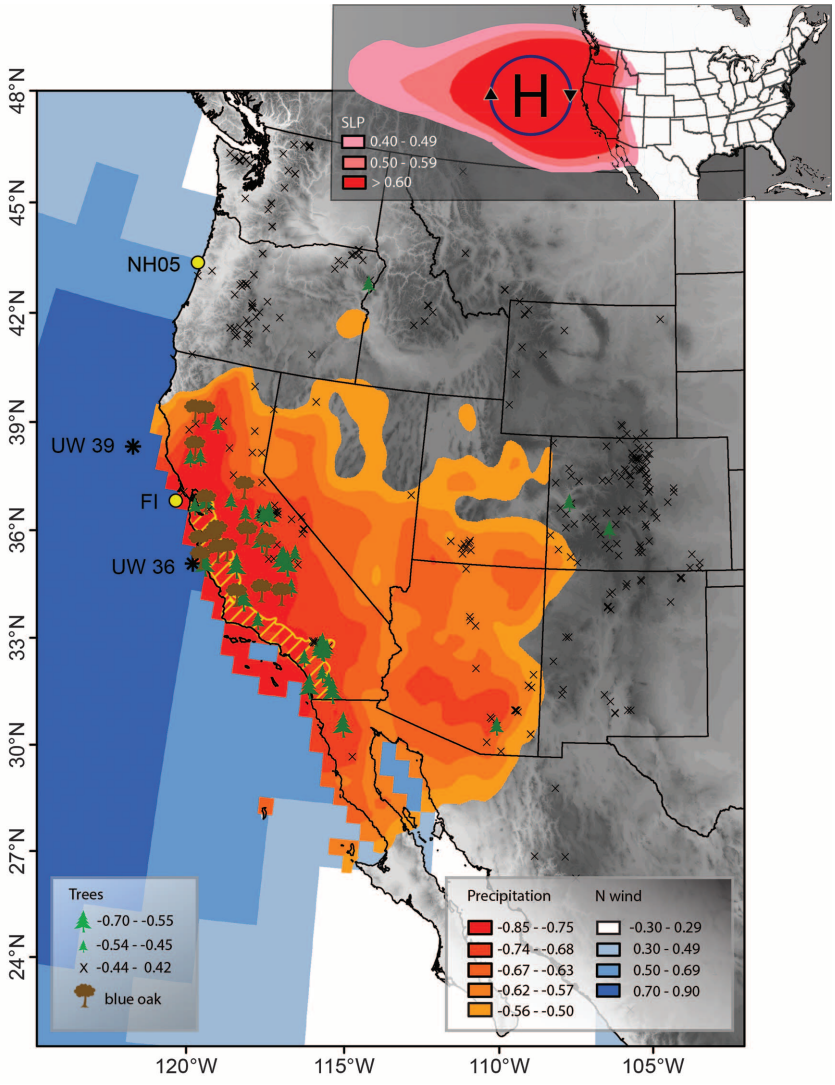

Fig. 1. Climate-driven linkages between marine and terrestrial ecosystems, as captured by the CCWI. (**Inset, top right**) Correlations (*r*) between winter SLP and the CCWI in the eastern North Pacific. High pressure (the NPH) blocks the onshore flow of winter storms, decreasing precipitation in the western United States. The clockwise rotation of these systems is associated with northwesterly upwelling-favorable winds. The main figure shows correlations between the CCWI and (i) gridded National Centers for Environmental Prediction/National Center for Atmospheric Research 1948–2010 winter meridional winds, where positive correlations indicate flow from the north (blue scaling); (ii) gridded Climatic Research Unit Time Series 3.1 winter precipitation on land (orange scaling); and (iii) tree-ring chronologies in western North America (green symbols). Also shown are the locations of the blue oak chronologies used in the CCWI reconstruction; upwelling stations at 36° and 39°N latitude (UW39 and UW36); the location of the Farallon Islands (FI) 48 km offshore from San Francisco, California (seabird data); and the locations of the Newport Hydrographic line station 5 (NH05; copepod data). The yellow hatched region represents NOAA NCDC Climate Divisions CA 04 and CA 06, from which precipitation data were obtained for the period 1895–2008 (fig. S1). All correlations in this figure involve an overlap of at least 40 years, but not more than 60 years.

[1]University of Texas Marine Science Institute, 750 Channel View Drive, Port Aransas, TX 78373, USA. [2]Farallon Institute for Advanced Ecosystem Research, 101 H Street, Suite Q, Petaluma, CA 94952, USA. [3]Swiss Federal Research Institute WSL, Zürcherstrasse 111, CH-8903 Birmensdorf, Switzerland and Oeschger Centre for Climate Change Research, University of Bern, Zähringerstrasse 25, CH-3012 Bern, Switzerland. [4]Department of Geology and Geophysics, Woods Hole Oceanographic Institution, 266 Woods Hole Road, Woods Hole, MA 02543, USA. [5]Department of Geosciences, University of Arkansas, 216 Ozark Hall, Fayetteville, AR 72701, USA. [6]Farallon Institute for Advanced Ecosystem Research, 101 H Street, Suite Q, Petaluma, CA 94952, USA. [7]Department of Biological Sciences and Marine Science Program, University of South Carolina, 701 Sumter Street, Columbia, SC 29208, USA. [8]Environmental Research Division, Southwest Fisheries Science Center, National Oceanic and Atmospheric Administration (NOAA), 1352 Lighthouse Avenue, Pacific Grove, CA 93950, USA. [9]Northwest Fisheries Science Center, Hatfield Marine Science Center, NOAA, 2030 Southeast Marine Science Drive, Newport, OR 97365, USA.
***Corresponding author. E-mail: bryan.black@utexas.edu**

vigorous fish growth, early seabird egg laying, and high seabird breeding success are all coincident with reduced tree growth (table S1). A large fraction of the interannual variability in $PC1_{bio}$ is explained by the CCWI [coefficient of determination (R^2) = 0.72; Fig. 2 and Table 1]. The stability of the relationship between these climate and biological variables is verified by the early interval of the rockfish growth chronology (R^2 = 0.56 with the CCWI for the 1948–1971 period; Fig. 2, B and C). The CCWI is also closely related to the leading principal component of a broader group (n = 9; 1982–2006) of CC seabird and fish time series (fig. S2) (*7*), as well as a regional zooplankton index for which positive anomalies indicate abundant cold-water, lipid-rich copepod species associated with high marine productivity (Fig. 2 and Table 1) (*12*). Such pervasive linkages across the ecosystem further substantiate the biological relevance of this wintertime climate indicator.

Given the tight relationships between marine and terrestrial ecosystems, we used the 16 blue oak chronologies to develop an ensemble-based reconstruction of winter upwelling climate back to 1428 CE (Fig. 3C; median R^2 = 0.58; Fig. 3A and table S4). The stability of this new reconstruction is verified by a median R^2 of 0.51 (P < 0.0001) between independent sea-level instrumental data (1898–1947) and each ensemble member (Fig. 3C and table S4). The reconstruction does not display long-term trends in the mean and is dominated by higher-frequency variability (<30 years; fig. S3), despite employing techniques capable of preserving interannual to centennial fluctuations in tree-ring data. In contrast, long-term trends are evident in variance, which increased sharply from approximately 1950 CE, (Fig. 3, B and D), which is consistent with observations of rising variability over recent decades in a number of CC biological time series (*13*). However, the multicentennial perspective afforded by winter climate reconstruction demonstrates that both the maximum variance and the rate of late–20th- and early–21st-century variance increase are high, but not unprecedented in the context of the past 600 years (Fig. 3D). Comparable levels in variance occurred during the mid–20th century and the latter 19th century, two peaks in an oscillating pattern that dates back to at least the mid-1600s. Additional instrumental records suggest that the late–20th-century rise in variance was particularly pronounced for precipitation (fig. S6) (*14*). The CCWI and associated winter variables correlate only weakly with the Pacific Decadal Oscillation (PDO), an important multidecadal mode of variability in the northeast Pacific (*15*) (table S1 and fig. S7). Establishing correspondence between the PDO and periods of high and low variance in the CCWI is hindered by the low number of PDO regime shifts in the instrumental record and the modest level of agreement among PDO reconstructions (fig. S7) (*16*).

Although our reconstruction indicates that modern winter climate variability is within historical bounds, the frequency of negative anomalies per century, as calculated for each ensemble member, is between three and five times greater after 1950 than before 1950 (Fig. 3F and table S5). This is of particular ecological significance, given that the relationship between the CCWI and $PC1_{bio}$ is nonlinear, so that negative CCWI values exert disproportionately severe impacts on marine biological functioning (Fig. 2A and fig. S2). Consequently, although rising wintertime variability over recent decades may not be unprecedented, it has

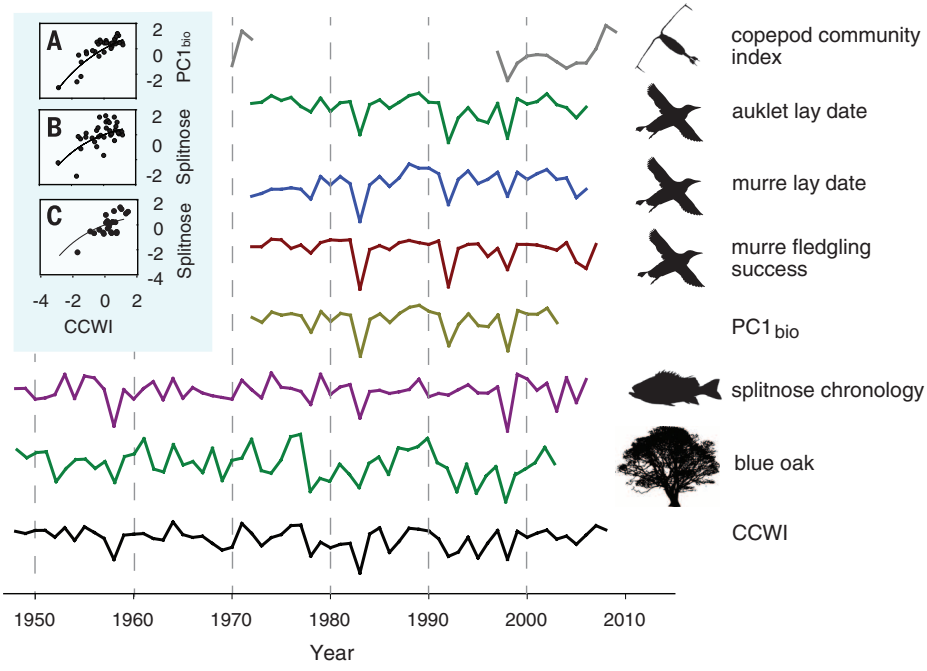

Fig. 2. The CCWI and its coherence with biological time series. Data sets shown are the winter copepod index, murre laying date, auklet laying date, murre fledgling success, a splitnose rockfish otolith chronology, and the mean of the 16 blue oak tree-ring chronologies used in the CCWI reconstruction. The leading principal component ($PC1_{bio}$) for all marine biological time series except copepods is also included. All time series are normalized, and the lay date, copepod, and blue oak time series are inverted to illustrate synchrony. (Inset) (**A**) Bivariate plot of CCWI and $PC1_{bio}$ (1973–2006; regression with an exponential rise to maximum function; R^2 = 0.72; P < 0.001). (**B**) Bivariate plot of CCWI and the latter portion of the splitnose chronology (1972–2006; regression with an exponential rise to maximum function; R^2 = 0.38; P < 0.001). (**C**) Bivariate plot of CCWI and the early portion of the splitnose chronology (1948–1971; regression with exponential rise to maximum function developed for late portion of the chronology; R^2 = 0.55; P < 0.001).

Table 1. Correlations among biological time series and the CCWI. Pearson correlation coefficients (r) and nominal P values (in italics; not corrected for autocorrelation) among marine biological time series, the CCWI, the mean of the 16 blue oak chronologies used in the CCWI reconstruction, and the CCWI tree-ring reconstruction.

Biological variable	CCWI*		CCWI reconstruction†		Blue oak‡		Time span§
Murre lay date	−0.66	*<0.001*	−0.42	*0.018*	0.37	*0.039*	1972–2006
Auklet lay date	−0.78	*<0.001*	−0.64	*<0.001*	0.58	*<0.001*	1972–2006
Murre success	0.57	*<0.001*	0.38	*0.035*	−0.34	*0.059*	1972–2006
Splitnose chronology	0.62	*<0.001*	0.41	*0.001*	−0.32	*0.015*	1948–2006
Winter copepod	−0.78	*<0.001*	−0.74	*0.015*	0.74	*0.014*	1970–1972; 1996–2010
$PC1_{bio}$‖	0.84	*<0.001*	0.67	N/A¶	−0.61	N/A¶	1972–2003

*The CCWI is the leading principal component of the winter Northern Oscillation Index, winter sea level at SFO, and winter upwelling index in the central CC. †Reconstruction of the CCWI from tree-ring data (ensemble median). ‡Mean of 16 blue oak chronologies used in the CCWI reconstruction. §Years spanned by the time series. ‖The leading principal component of murre laying date, auklet laying date, murre fledgling success, the splitnose rockfish otolith growth-increment chronology, and the mean of 16 blue oak chronologies. ¶Level of significance is not applicable; the blue oak mean is used in calculating $PC1_{bio}$ and the reconstructed CCWI.¶

been driven by a succession of winters with anomalously low SLP over the northeast Pacific, each of which profoundly reduced fish growth and seabird productivity (Figs. 2A and 3F). The frequency of positive, upwelling-favorable, winter climate anomalies does not differ before and after 1950 (table S6), underscoring the role of negative (downwelling-favorable) anomalies in driving the rise of late–20th-century variability.

Winter climate extremes along the western North American coast are teleconnected to the El Niño–Southern Oscillation (ENSO). Forty-two percent of the variance in the CCWI is explained by the mean Jan-Mar Multivariate ENSO Index, and four of the most negative reconstructed CCWI values (1998, 1983, 1941, and 1868) correspond to major El Niño events (*17*) (Fig. 3). ENSO reconstructions indicate that the 20th century was highly variable in the context of the past centuries (*18*–*20*) or even millennia (*21*), which could explain, at least in part, rising variance in the CCWI. Linkages between anthropogenic climate change and rising ENSO variability remain unclear, and models of future ENSO behavior have not yet reached consensus (*22*). Thus, CC winter climate trends cannot be easily attributed or forecast. However, the importance of these patterns is clear in the CC and adjacent forests, with implications for biological processes beyond those examined here. For example, rising variance in average cool-season precipitation probably hastened the recent extinction of two checkerspot butterfly (*Euphydryas editha bayensis*) populations in the San Francisco Bay Area (*23*). Moreover, blocking high pressure (strong NPH) and associated drought, snowpack deficits, low river flows, and elevated wildfire risks in early 2013 and now 2014, illustrate the importance of winter climate to agriculture, ecosystems, water security, and even hydroelectric power generation in central and southern California, a region where freshwater resources are currently overallocated, so that any reductions in rainfall cause conflict over this valuable resource. Although the temporal resolution of this tree-ring reconstruction is well suited to identifying these high-frequency patterns, other proxies with greater temporal depth, such as sedimentary records, demonstrate that western North American coastal precipitation, and possibly winter upwelling, was highly dynamic over the course of the Holocene (*24*, *25*). Extremely low-frequency, multicentennial fluctuations at time scales exceeding those considered here may an important component of the winter climate system.

Owing to strong linkages with terrestrial productivity, we were able to generate an annually resolved multicentennial reconstruction of CC wintertime climate that reflects marine biological functioning in a coastal ecosystem. Such a highly targeted tree-ring approach may be possible in other coupled systems, especially eastern boundary upwelling zones, assuming that regional climate drivers of productivity have been identified and are linked to atmospheric processes that influence forest growth. Depending on the seasonality of biological response, trees may

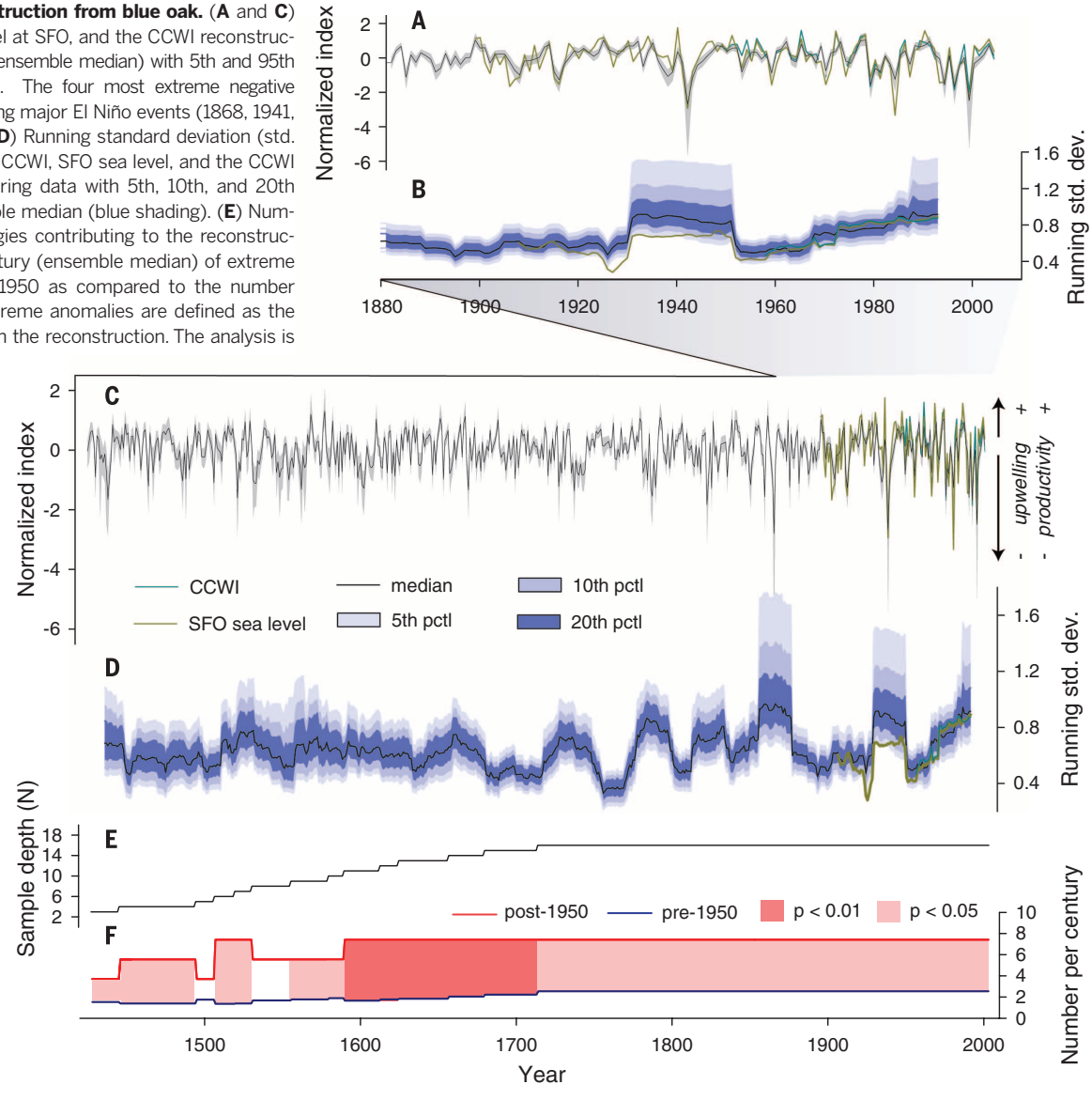

Fig. 3. The CCWI reconstruction from blue oak. (**A** and **C**) The CCWI, winter sea level at SFO, and the CCWI reconstruction from tree-ring data (ensemble median) with 5th and 95th percentiles (gray shading). The four most extreme negative estimates all occurred during major El Niño events (1868, 1941, 1983, and 1998). (**B** and **D**) Running standard deviation (std. dev.) (21-year window) of CCWI, SFO sea level, and the CCWI reconstruction from tree-ring data with 5th, 10th, and 20th percentiles of the ensemble median (blue shading). (**E**) Number of blue oak chronologies contributing to the reconstruction. (**F**) Number per century (ensemble median) of extreme negative anomalies post-1950 as compared to the number per century pre-1950. Extreme anomalies are defined as the 10 most negative values in the reconstruction. The analysis is repeated at each change in reconstruction sample depth to illustrate that pre- and post-1950 differences persist, even where the number of contributing chronologies is low and the time period constituting "pre-1950" is longest (i.e., 1428–1950 at a sample depth of 3 versus 1714–1950 at a sample depth of 16). Pink shading indicates a significant difference pre- and post-1950. See table S5 for values.

also capture signals of warm-season upwelling, which in the CC is uncorrelated to winter upwelling and dominated by decadal-scale variability (*3*, *5*, *26*). Overall, multivariable indices such as those we developed and describe here highlight broad physical-ecological connections and may provide new options for monitoring and "hindcasting" ecosystem states. In this example, covariance among fish, seabirds, and trees demonstrates a remarkable degree of connectivity across the coastal interface that not only provides context for interpreting variability in observational records but may also be relevant to management. Identifying biologically important indicators, their current status, and their ranges of historical variability is central to the desired transition from single-species fisheries stock assessments to the next generation of integrative ecosystem-based strategies (*27*).

REFERENCES AND NOTES

1. A. Huyer, *Prog. Oceanogr.* **12**, 259–284 (1983).
2. R. L. Smith, *Oceanogr. Mar. Biol. Annu. Rev.* **6**, 11–46 (1968).
3. W. J. Sydeman *et al.*, *Science* **345**, 77–80 (2014).
4. B. A. Black, *Mar. Ecol. Prog. Ser.* **378**, 37–46 (2009).
5. B. A. Black *et al.*, *Glob. Change Biol.* **17**, 2536–2545 (2011).
6. I. D. Schroder *et al.*, *Geophys. Res. Lett.* **40**, 1–6 (2013).
7. M. García-Reyes *et al.*, *Ecosystems (N.Y.)* **16**, 722–735 (2013).
8. S. St George, D. M. Meko, E. R. Cook, *Holocene* **20**, 983–988 (2010).
9. F. B. Schwing, T. Murphree, P. M. Green, *Prog. Oceanogr.* **53**, 115–139 (2002).
10. F. B. Schwing, M. O'Farrell, J. M. Steger, K. Baltz, "Coastal upwelling indices, West Coast of North America, 1946-1995," *NOAA Technical Memo, NOAA-TM-NMFS-SWFSC* (NOAA, Washington, DC, 1996).
11. D. W. Stahle *et al.*, *Earth Interact.* **17**, 1–23 (2013).
12. J. E. Keister, E. Di Lorenzo, C. A. Morgan, V. Combes, W. T. Peterson, *Glob. Change Biol.* **17**, 2498–2511 (2011).
13. W. J. Sydeman, J. A. Santora, S. A. Thompson, B. M. Marinovic, E. Di Lorenzo, *Glob. Change Biol.* **19**, 1662–1675 (2013).
14. A. F. Hamlet, D. P. Lettenmaier, *Water Resour. Res.* **43**, W06427 (2007).
15. N. J. Mantua, S. R. Hare, Y. Zhang, J. M. Wallace, R. C. Francis, *Bull. Am. Meteorol. Soc.* **78**, 1069–1079 (1997).
16. K. F. Kipfmueller, E. R. Larson, S. St George, *Geophys. Res. Lett.* **39**, L21705 (2012).
17. K. Wolter, M. S. Timlin, *Weather* **53**, 315–324 (1998).
18. J. B. Li *et al.*, *Nat. Clim. Change* **1**, 114–118 (2011).
19. D. W. Stahle *et al.*, *Bull. Am. Meteorol. Soc.* **79**, 2137–2152 (1998).
20. A. M. Fowler *et al.*, *Nat. Clim. Change* **2**, 172–176 (2012).
21. K. M. Cobb *et al.*, *Science* **339**, 67–70 (2013).
22. M. Collins *et al.*, *Nat. Geosci.* **3**, 391–397 (2010).
23. J. F. McLaughlin, J. J. Hellmann, C. L. Boggs, P. R. Ehrlich, *Proc. Natl. Acad. Sci. U.S.A.* **99**, 6070–6074 (2002).
24. N. E. Graham *et al.*, *Clim. Change* **83**, 241–285 (2007).
25. F. P. Malamud-Roam, B. L. Ingram, M. Hughes, J. L. Florsheim, *Quat. Sci. Rev.* **25**, 1570–1598 (2006).
26. F. B. Schwing, R. Mendelssohn, *J. Geophys. Res. Oceans* **102**, 3421–3438 (1997).
27. P. S. Levin, M. J. Fogarty, S. A. Murawski, D. Fluharty, *PLOS Biol.* **7**, e1000014 (2009).

ACKNOWLEDGMENTS

Funding was provided by NSF (grant no. 1130125), the NOAA Fisheries and the Environment (FATE) program, the California Department of Fish and Wildlife Ecosystem Restoration Program (grant no. ERP02-P30), and the Nippon Foundation-University of British Columbia Nereus Program. D.G. was supported by a NOAA Climate and Global Change Postdoctoral Fellowship. Seabird data were obtained from Point Blue Conservation Science/Farallon National Wildlife Refuge. We are grateful to contributors to the International Tree-Ring Databank and thank M. O'Connor for assistance with Fig. 1. Finally, we thank the reviewers for their comments and insights, which greatly improved the paper. All data used in this work, or the sources from which they are available, are included in the supplementary materials.

SUPPLEMENTARY MATERIALS

www.sciencemag.org/content/345/6203/1498/suppl/DC1
Materials and Methods
Figs. S1 to S7
Tables S1 to S6
References (*28*–*30*)

11 March 2014; accepted 7 August 2014
10.1126/science.1253209

SOCIAL SCIENCE

Publication bias in the social sciences: Unlocking the file drawer

Annie Franco,[1] Neil Malhotra,[2]* Gabor Simonovits[1]

We studied publication bias in the social sciences by analyzing a known population of conducted studies—221 in total—in which there is a full accounting of what is published and unpublished. We leveraged Time-sharing Experiments in the Social Sciences (TESS), a National Science Foundation–sponsored program in which researchers propose survey-based experiments to be run on representative samples of American adults. Because TESS proposals undergo rigorous peer review, the studies in the sample all exceed a substantial quality threshold. Strong results are 40 percentage points more likely to be published than are null results and 60 percentage points more likely to be written up. We provide direct evidence of publication bias and identify the stage of research production at which publication bias occurs: Authors do not write up and submit null findings.

Publication bias occurs when "publication of study results is based on the direction or significance of the findings" (*1*). One pernicious form of publication bias is the greater likelihood of statistically significant results being published than statistically insignificant results, holding fixed research quality. Selective reporting of scientific findings is often referred to as the "file drawer" problem (*2*). Such a selection process increases the likelihood that published results reflect type I errors rather than true population parameters, biasing effect sizes upwards. Further, it constrains efforts to assess the state of knowledge in a field or on a particular topic because null results are largely unobservable to the scholarly community.

Publication bias has been documented in various disciplines within the biomedical (*3*–*9*) and social sciences (*10*–*17*). One common method of detecting publication bias is to replicate a meta-analysis with and without unpublished literature (*18*). This approach is limited because much of what is unpublished is unobserved. Other methods solely examine the published literature and rely on assumptions about the distribution of unpublished research by, for example, comparing the precision and magnitude of effect sizes among a group of studies. In the presence of publication bias, smaller studies report larger effects in order to exceed arbitrary statistical significance thresholds (*19*, *20*). However, these visualization-based approaches are sensitive to using different measures of precision (*21*, *22*) and also assume that outcome variables and effect sizes are comparable across studies (*23*). Last, methods that compare published studies to "gray" literatures (such as dissertations, working papers, conference papers, or human subjects registries) may confound strength of results with research quality (*7*). These techniques are also unable to determine whether publication bias occurs at the editorial stage or during the writing stage. Editors and reviewers may prefer statistically significant results and reject sound studies that fail to reject the null hypothesis. Anticipating this, authors may not write up and submit papers that have null findings. Or, authors may have their own preferences to not pursue the publication of null results.

A different approach involves examining the publication outcomes of a cohort of studies, either prospectively or retrospectively (*24*, *25*). Analyses of clinical registries and abstracts submitted to medical conferences consistently find little to no editorial bias against studies with null findings (*26*–*31*). Instead, failure to publish appears to be most strongly related to authors' perceptions that negative or null results are uninteresting and not worthy of further analysis or publication (*32*–*35*). One analysis of all institutional review board–approved studies at a single university over 2 years found that a majority of conducted research was never submitted for publication or peer review (*36*).

Surprisingly, similar cohort analyses are much rarer in the social sciences. There are two main reasons for this lacuna. First, there is no process in the social sciences of preregistering studies

[1]Department of Political Science, Stanford University, Stanford, CA, USA. [2]Graduate School of Business, Stanford University, Stanford, CA, USA.
*Corresponding author. E-mail: neilm@stanford.edu